ORIGINAL PAPER

Resonances of a forced van der Pol equation with parametric damping

Fatemeh Afzali · **Ehsan Kharazmi** ·
Brian F. Feeny

Abstract This work entails an analysis of secondary resonances in the parametrically damped van der Pol equation, with and without external excitation. A potential application of this system is a vertical-axis wind-turbine blade, which can have cyclic damping, aeroelastic self-excitation, and direct excitation. We analyze the system using the method of multiple scales and numerical solutions. For the case without external excitation, the analysis reveals nonresonant phase drift (quasiperiodic responses) and subharmonic resonance with possible phase drift or phase locking (periodic responses). The case of external excitation consists of a constant load and a harmonic load with the same frequency as the parametric term. Hard excitation is treated for nonresonant conditions and secondary resonances. Subharmonic and superharmonic resonances show possible phase drift and phase locking. Primary resonance is observed but not analyzed here.

F. Afzali (✉) · B. F. Feeny
Michigan State University, East Lansing, MI 48824, USA
e-mail: :afzalifa@msu.edu

E. Kharazmi
Brown University, Providence, RI 02912, USA

1 Introduction

In this paper, we study the responses of an oscillator with van der Pol terms, parametric damping and direct excitation. A potential application of this system is a vertical-axis wind-turbine blade, which can endure direct excitation and parametric damping [1,2], as well as aeroelastic self-excitation, the effects of which can be loosely modeled with van der Pol nonlinearity [3,4]. Here, the general behavior of this system is studied, rather than the specific responses of a specific model of an application system. As both parametric excitation and van der Pol nonlinearity can induce instabilities and oscillations, we seek to understand the combined effect of such terms in this system.

The nonlinear damping in the van der Pol equation was originally introduced to model electrical oscillations [5]. This nonlinearity is well known to induce limit-cycle oscillations. Holmes and Rand [6] studied the bifurcation of the variational equation of the forced van der Pol oscillator. Barbosa et al. [7] studied the modified version of the classical van der Pol oscillator containing derivatives of fractional order. They applied approximations to fractional-order operators to show the dynamics of the model through numerical simulations. Náprstek and Fischer [8] assessed the original sub- and supersynchronization effects and their dynamic stability in a generalized van der Pol oscillator. Barron and Sen [9] investigated the synchronization of four coupled van der Pol oscillators representing the

synchronization of the self-excited vibrations in turbo-machine blades due to elastic coupling.

Parametric excitation also induces significant behavior in dynamical systems and therefore has been of keen interest, in particular through the Mathieu equation [3,4,10] in the context of parametric stiffness. Parametric damping has been shown to generate instabilities [2,11] similar to those of the Mathieu equation [3,4] with period-1 or period-2 oscillation, and to decay with quasiperiodic dynamics when stable [2], the latter shown by combining the Floquet solution with a harmonic balance [12,13].

There have been vast studies on related systems that consider parametric excitation and/or direct excitation with and without nonlinearity. Examples include Mathieu oscillators without forcing [14–17], with forcing [18–24], and a Mathieu–van der Pol system [25]. Pandey et al. [26] inquired into frequency locking in a forced Mathieu–van der Pol–Duffing system near the principal resonances with the application of optically actuated MEMS resonators. Belhaq and Fahsi [27] examined the effect of a fast harmonic parametric excitation on frequency-locking in 2:1 and 1:1 resonances in a similar system.

Szabelski and Warminski [28] analyzed systems with three sources of vibration: parametric, self-excited and external. Warminski [29] studied the nonlinear dynamics of a self-, parametric, and externally excited oscillator with time delay by applying the method of multiple scales. Similar to the current paper, Chakraborty and Sarkar [30] studied the parametrically excited van der Pol oscillator with a modified nonlinear damping term. They presented resonance and anti-resonance effects using an approach for bookkeeping slowly varying amplitudes and small terms. They also illustrated that coupling between two van der Pol oscillators can be applied as a binary switch.

Parametric excitation has also been studied in the context of wind turbine blades [21,22,31,32]. Luongo and Zulli [33] studied a self-excited tower under turbulent wind flow. The tower was assumed to be a nonlinear system where the mean wind led to self excitation and the turbulent part caused parametric and external excitation.

In this study, we combine parametric damping with self-excitation of a van der Pol equation. With a partic-ular choice of scaling and excitation frequencies, the equation becomes

$$
\begin{aligned}
&\ddot{x} + \epsilon(c_0 + c_1 \cos \omega t + \alpha x^2)\dot{x} \\
&+ \omega_n{}^2 x = f_0 + f_1 \sin(\omega t),
\end{aligned}
\tag{1}
$$

where $\epsilon \ll 1$. The variables c_0 and c_1 are the scaled mean damping and amplitude of the parametric damping, respectively, and f_0 and f_1 are mean and cyclic direct excitation constants. The excitation frequency is ω and the linearized natural frequency is ω_n. We will refer to this as the parametrically damped van der Pol (PDVDP) equation with external excitation. We apply the first-order method of multiple scales [3,34] to study the unforced and externally forced cases with parametric damping at frequency ω.

In Sect. 2, we set up the analysis using the method of multiple scales. In Sect. 3, we analyze the case without external excitation, where we consider the nonresonant case and subharmonic resonance of order 1/2. In Sect. 4, we study the system with both parametric and external excitation, where in addition to previous resonance cases, we also analyze the superharmonic resonance of order 2. We provide a brief comment on the strength of nonlinearity in Sect. 5 and concluding remarks in Sect. 6.

2 Perturbation analysis: method of multiple-scales

The core of this study is the approximation of the solution to Eq. (1) based on the method of multiple scale (MMS) [3,4]. We expand the displacement as $x(T_0, T_1, \ldots) = x_0(T_0, T_1, \ldots) + \epsilon x_1(T_0, T_1, \ldots) + \epsilon^2 x_2(T_0, T_1, \ldots) + \cdots$, where the time scales are $T_i = \epsilon^i t$, and $\epsilon \ll 1$. By using the chain rule, we obtain the derivatives for $n \in \mathbb{N}$ as $\frac{d^n}{dt^n}(\cdot) = (D_0 + \epsilon D_1 + \epsilon^2 D_2 + \cdots)^n(\cdot)$, where $D_i = \frac{\partial}{\partial T_i}$. Here, we carry out the analysis up to the first order by considering the two time scales $T_0 = t$ and $T_1 = \epsilon t$ and therefore expand the displacement as

$$
x(T_0, T_1) \approx x_0(T_0, T_1) + \epsilon x_1(T_0, T_1). \tag{2}
$$

By substituting the expansion (2) in Eq. (1) and using the derivatives, coefficients of similar powers of ϵ equate as

$$\epsilon^0 : D_0^2 x_0 + \omega_n^2 x_0 = f_0 + f_1 \sin(\omega T_0), \qquad (3)$$

$$\epsilon^1 : D_0^2 x_1 + \omega_n^2 x_1$$
$$= -2D_0 D_1 x_0 - (c_0 + c_1 \cos \omega T_0 + \alpha x_0^2)(D_0 x_0). \qquad (4)$$

The relationship between the excitation and the natural frequencies specifies different cases of resonance.

1. Nonresonant: no specific relationship between ω and ω_n
2. Primary resonance: $\omega \approx \omega_n$
3. Superharmonic resonance: $\omega \approx \omega_n/2$
4. Subharmonic resonance: $\omega \approx 2\omega_n$

In the next sections, we elaborate on this perturbation analysis for specific cases without and with external excitation and apply other tools to examine the dynamics with emphasis on secondary resonances.

3 Parametric excitation without external excitation

We start with the case where there is no external forcing, i.e., $f_0 = f_1 = 0$. As a survey of the possible dynamics, Fig. 1 shows a frequency sweep from $\omega = 0$ to beyond $\omega = 2\omega_n$, when $\omega_n = 1$, $\epsilon = 0.1$, $c_0 = -1$, and $c_1 = 1$ (these parameters are dimensionless). The sweep, as a bifurcation diagram, represents samples of the x variable of the nonwandering set in a Poincaré section [35] for various values of the frequency parameter. A Runge–Kutta method (Matlab ode45) is used to obtain numerical solutions at each frequency over many periods to approach steady state. As the responses are typically quasiperiodic, the plots are generated by recording 50 values of x at the downward $\dot{x} = 0$ crossing in the phase space for each excitation frequency. Thus the points in the plot represent local maxima in $x(t)$.

The plot shows that significant quasiperiodic dynamics occur for a large range of excitation frequencies, with a periodic window around $\omega \approx 2\omega_n$. The largest responses occur near this subharmonic range and also the low frequencies. Superharmonic and primary resonances are not apparent beyond a possible frequency interval of periodic or nearly periodic dynamics. Figure 2 shows examples of quasiperiodic responses for three different excitation frequencies.

We appeal to perturbation analysis to explain these responses. The solution to the zeroth order Eq. (3) with

$f_0 = 0$ and $f_1 = 0$ is

$$x_0(T_0, T_1) = A(T_1)e^{i\omega_n T_0} + c.c., \qquad (5)$$

where $c.c.$ stands for the corresponding complex conjugate terms. We obtain the solvability conditions by substituting Eq. (5) into the right-hand side of Eq. (4) and eliminating the secular terms, which are the terms that make the solution to x_1 grow without bound in time, and thus should be eliminated. By plugging Eq. (5) into (4), we obtain

$$D_0^2 x_1 + \omega_n^2 x_1 = (-2i\omega_n A' - ic_0\omega_n A$$
$$- \alpha i \omega_n A^2 \bar{A})e^{i\omega_n T_0}$$
$$+ \frac{c_1}{2}\left(i\omega_n \bar{A}e^{i(\omega-\omega_n)T_0}\right) + c.c. + \text{N.S.T.}, \qquad (6)$$

where N.S.T. stands for non-secular terms, and $A' = D_1 A$. The homogeneous solution of Eq. (6) is of the form $e^{i\omega_n T_0}$. Therefore any right-hand side term that is of the same frequency will become secular and cause x_1 to grow without bound.

We seek the resonance cases that lead to additional secular terms. The right-hand side of Eq. (6) merely shows a subharmonic resonance case. However, as shown in Fig. 1 as well as Eq. (6), the system has significant oscillatory behavior at the nonresonant case, that is when there is no specific relationship between the excitation frequency ω and the natural frequency ω_n. The solvability conditions for these two cases are as follows.

- Nonresonant:

$$2A' + c_0 A + \alpha A^2 \bar{A} = 0 \qquad (7)$$

- Subharmonic resonance of order 1/2 ($\omega = 2\omega_n + \epsilon\sigma$):

$$2A' + c_0 A + \alpha A^2 \bar{A} - \frac{c_1}{2}\bar{A}e^{i\sigma T_1} = 0 \qquad (8)$$

where σ is a detuning parameter.

3.1 Nonresonant case

We first consider the nonresonant case, where the solvability condition takes the form $2A' + c_0 A + \alpha A^2 \bar{A} = 0$. We recall that A is a complex function of T_1. Writing it as $A(T_1) = \frac{1}{2}a(T_1)e^{i\beta(T_1)}$, the solvability condition becomes

$$a' + ia\beta' + \frac{1}{2}c_0 a + \frac{1}{8}\alpha a^3 = 0. \qquad (9)$$
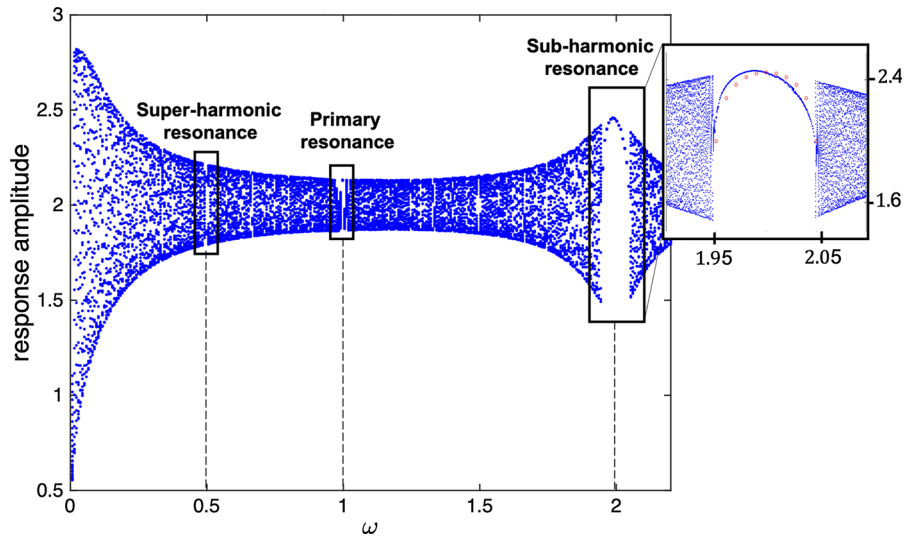
Fig. 1 PDVDP with parametric excitation only. The numerically solved response amplitude versus the excitation frequency when $f_0 = f_1 = 0$, $\omega_n = 1$, $\epsilon = 0.1$, $c_0 = -1$, $c_1 = 1$, and $\alpha = 1$. The embedded subplot zooms in on the strong subharmonic resonance window. The circles are amplitudes predicted by the perturbation analysis

By separating the real and imaginary parts, we obtain the following governing equations of amplitude a and phase β as

$$a' + \frac{1}{2}c_0 a + \frac{1}{8}\alpha a^3 = 0, \quad a\beta' = 0. \tag{10}$$

The response amplitude has steady-state values, obtained by setting $a' = 0$, that depend on the parameter c_0. When $c_0 < 0$, there is a stable steady-state amplitude of $a = 2\sqrt{\frac{-c_0}{\alpha}}$. This amplitude and the solvability condition that leads to it are the same as in the regular van der Pol equation when $c_0 = -1$. By eliminating the solvability condition, we keep the remaining terms in Eq. (6) and find the particular solution to be

$$x_1 = Q_1 e^{3i\omega_n T_0} + Q_2 e^{i(\omega + \omega_n)T_0} + Q_3 e^{i(\omega_n - \omega)T_0}, \tag{11}$$

where

$$Q_1 = \frac{\alpha i A^3}{8\omega_n}, \quad Q_2 = \frac{c_1 i \omega_n A}{2\omega(\omega + 2\omega_n)},$$
$$Q_3 = \frac{c_1 i \omega_n A}{2\omega(\omega - 2\omega_n)}, \tag{12}$$

in which $A = \frac{1}{2}a e^{i\beta}$. We note that Eq. (11) is valid if $\omega \neq 2\omega_n$. Then the leading-order nonresonant solution is

$$x = x_0 + \epsilon x_1 = a\cos(\omega_n T_0 + \beta)$$

$$+ \epsilon(2Q_1 \cos(3\omega_n T_0) + 2Q_2 \cos(\omega + \omega_n)T_0$$
$$+ 2Q_3 \cos(\omega - \omega_n)T_0). \tag{13}$$

This result for the nonresonant case demonstrates a uniformly present oscillation term at the amplitude a that comes from the van der Pol element, plus small oscillatory parametric terms with frequency-dependent amplitudes, and with two independent frequencies, such that in typical cases the result is quasiperiodic.

The numerical solutions in Fig. 2 have features described by the nonresonant case. When $\omega = 0.12$, the response looks like classic beating that can arise with the sum of two incommensurate simple harmonics. This is consistent with the approximate solution in Eq. (13). The cases of $\omega = 1.93$ and $\omega = 2.055$ provide bookends around the subharmonic resonance formulated in the next section. While the two latter cases seem to have features of the nonresonant solution, we will see that the subharmonic resonance analysis describes them more accurately.

3.2 Subharmonic resonance of order 1/2

Here, we focus on the subharmonic resonance case, where the excitation frequency is tuned to be close to twice the natural frequency, i.e., $\omega = 2\omega_n + \epsilon\sigma$. In this setting, the solvability condition is comprised of an additional term and is given as $2A' + c_0 A + \alpha A^2 \bar{A} -$
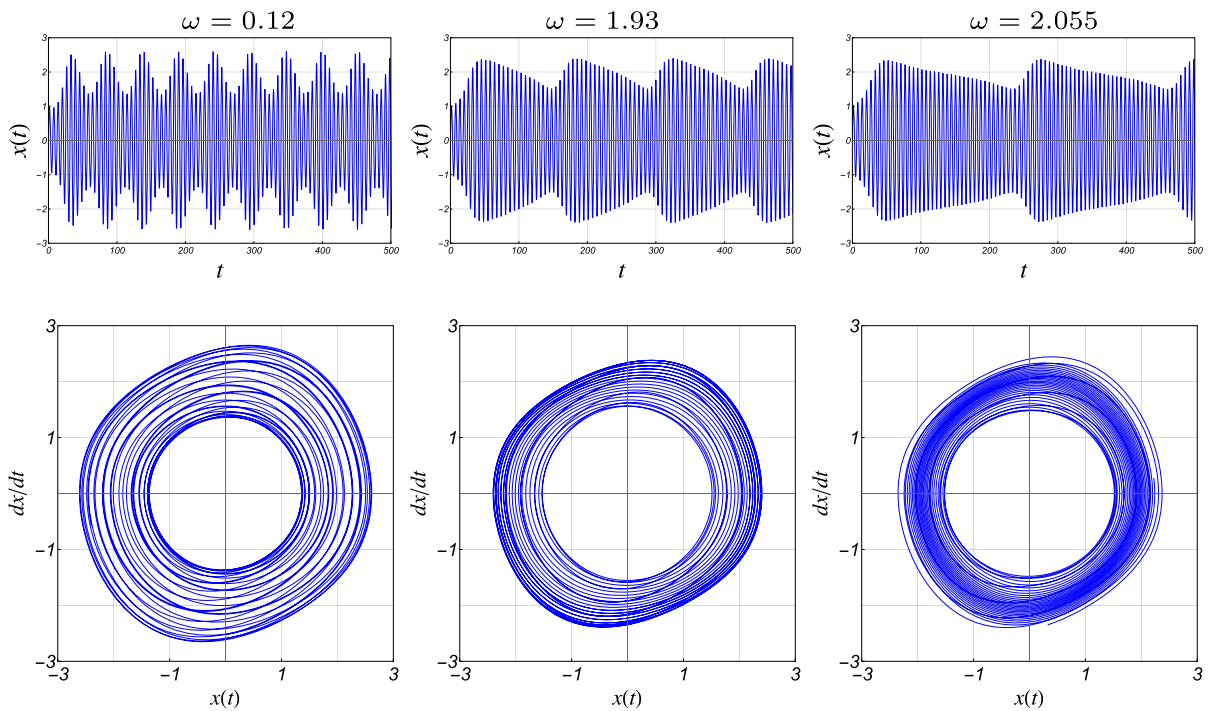
Fig. 2 PDVDP with parametric excitation only. The numerically solved time response (top row) and phase portrait (bottom row) at different excitation frequencies where $f_0 = f_1 = 0$, $\omega_n = 1$, $\epsilon = 0.1$, $c_0 = -1$, $c_1 = 1$, and $\alpha = 1$

$\frac{c_1}{2}\bar{A}e^{i\sigma T_1} = 0$. By letting $A(T_1) = \frac{1}{2}a(T_1)e^{i\beta(T_1)}$, we obtain

$$a' + ia\beta' + \frac{1}{2}c_0 a + \frac{1}{8}\alpha a^3 - \frac{1}{4}c_1 a e^{i(\sigma T_1 - 2\beta)} = 0. \tag{14}$$

We separate the real and imaginary parts and obtain the following governing equations

$$a' + \frac{1}{2}c_0 a + \frac{1}{8}\alpha a^3 - \frac{1}{4}c_1 a \cos(\sigma T_1 - 2\beta) = 0,$$
$$a\beta' - \frac{1}{4}c_1 a \sin(\sigma T_1 - 2\beta) = 0. \tag{15}$$

To investigate the dynamics of Eq. (15), we first make the system autonomous via the change of variables $\gamma = \sigma T_1 - 2\beta$ to obtain

$$a' + \frac{1}{2}c_0 a + \frac{1}{8}\alpha a^3 - \frac{1}{4}c_1 a \cos\gamma = 0,$$
$$a\gamma' + \frac{1}{2}c_1 a \sin\gamma - \sigma a = 0. \tag{16}$$

The response amplitude has steady-state values, obtained by setting $a' = \gamma' = 0$, that depend on the parameters c_0 and c_1. By using the trigonometric identities, we

remove γ and finally obtain the response amplitude as

$$a = 0, \quad \text{or} \tag{17}$$

$$\alpha a^2 = -4c_0 \pm 4\sqrt{\frac{c_1^2}{4} - \sigma^2}. \tag{18}$$

The nonzero solutions in Eq. (18) form an ellipse in (a^2, σ) space. If $\frac{c_1^2}{4} - \sigma^2 > 0$, and the right-hand side of Eq. (18) is positive, then there are both zero and non-zero real-valued response amplitudes. Otherwise, the only steady-state amplitude is zero.

Figure 3 shows the steady-state amplitude versus the excitation frequency $\omega = 2\omega_n + \epsilon\sigma$ for different values of c_0 and c_1 where $\epsilon = 0.1$, $\omega_n = 1$, and $\alpha = 1$. As the frequency increases, fixed points in a (periodic system responses) emerge at a critical value of ω that depends on c_1 ($\omega \approx 1.95$ for $c_1 = 1$), and stable solutions follow the upper branch (stability is addressed below). The amplitude a is maximum at $\omega = 2$ and the solution disappears at another critical ω ($\omega \approx 2.05$ for $c_1 = 1$). In the left panel in Fig. 3, when $c_0 = -1$, a larger amplitude of parametric damping c_1 leads to a larger response amplitude. The inner and outer ovals are associated with $c_1 = 0.2$ and $c_1 = 1$, respectively. An increase in

the mean value of damping c_0, however, decreases the response amplitude by pushing down the oval-shaped curve. In the right panel, at $c_0 = 0.5$, the oval disappears at the frequency of $\omega = 2$. When $c_0 \geq 0.5$, a^2 has only negative values and therefore no real nonzero solution exists.

Examples of analytical solution amplitudes from Eq. (18) are plotted as circles in the subharmonic insert in Fig. 1 for comparison with the numerical solutions. The pattern of the responses described here and shown in this insert are somewhat similar to those seen in [26] with parametric stiffness at subharmonic resonance, although that case has the influence of a direct excitation of half the frequency, and a cubic stiffness as well. The system of [30] also exhibits subharmonic periodic solutions surrounded by quasiperiodic behavior, but the structure of the slow flow near $\omega = 2$ is rather different.

3.2.1 Stability analysis

Stability of the steady-state solutions in Eq. (18) is determined from the Jacobian of Eqs. (16), given by

$$\begin{bmatrix} -\frac{1}{4}\alpha a^2 & -\frac{1}{2}a\sigma \\ 0 & -(c_0 + \frac{1}{4}\alpha a^2) \end{bmatrix} \qquad (19)$$

which has trace $T = -c_0 - \alpha\frac{a^2}{2}$ and determinant $D = \frac{1}{4}\alpha a^2(c_0 + \frac{\alpha a^2}{4})$. Here, a represents the equilibrium amplitude. A fixed point (steady-state amplitude a) is stable if $D > 0$, i.e., $\alpha a^2 + 4c_0 > 0$ (α is a positive number), and $T < 0$, i.e., $\alpha a^2 + 2c_0 > 0$. Thus, based on Eq. (18), if $\frac{c_1^2}{4} - \sigma^2 > 0$, then the nonzero fixed point exists and the $D > 0$ criterion implies that the positive (upper) branch is stable, while the lower branch is unstable. The $a = 0$ solution is neutrally stable if $c_0 > 0$. If $\frac{c_1^2}{4} - \sigma^2 > 0$, then fixed point defined by $\alpha a^2 = -4c_0 + 4\sqrt{\frac{c_1^2}{4} - \sigma^2}$ is stable.

3.2.2 Dynamics of the amplitude and phase

Figure 4 shows the stable and unstable branches (schematic) of the steady-state response amplitude (top panel), and the amplitude-phase trajectories (bottom panel) at the set of frequencies $\omega = \{1.93, 1.98, 2, 2.04, 2.05, 2.055\}$. The parameters are set to be $\epsilon = 0.1$, $\omega_n = 1$, $c_0 = -1$, $c_1 = 1$, and $\alpha = 1$. The upper panel shows that between frequencies of $\omega = 1.95$ and $\omega = 2.05$, there exist two steady-state response

amplitudes a, one on each branch of the oval-shaped curve. For $\omega < 1.95$ and $\omega > 2.05$, there are no nonzero fixed points. However, note that Eqs. (16) exist on a cylindrical state space, and for these frequency ranges they admit a "whirling" solution, whose mean is approximated in the top panel. Examples of whirling are depicted in the the lower panels for $\omega = 1.93$ for which the whirling solution travels from right to left, and for $\omega = 2.055$, for which the whirling solution travels from left to right. As such, the amplitude a of the leading order solution has a periodic fluctuation, and the oscillator is quasiperiodic, as labeled in the top panel of Fig. 4.

As ω increases, two fixed points in (a, γ) are created in a saddle-node bifurcation at $\omega = 1.95$. Likewise, when the frequency reaches $\omega = 2.05$, the two fixed points in (a, γ) collide and disappear in another saddle-node bifurcation. Panel 2 shows the two fixed points after the first saddle-node bifurcation. With increasing frequency, the saddle moves to the left, while the stable node moves to the right. In panel 3, at $\omega = 2.0$, the stable node has $\gamma = 0$ while the saddle has $\gamma = \pm\pi/2$ and is visible at both sides of the slice of the cylindrical phase space. In panel 4, the saddle and node have continued their trek to the left and right, respectively, and they are now approaching each other. In panel 5, at $\omega = 2.05$, the second saddle-node bifurcation has been reached, and the two fixed points coalesce. Panel 6 then shows whirling trajectories after the second saddle-node bifurcation.

Some information about the whirling orbits can be gleaned from Eqs. (16) when $\alpha = 1$. These equations have a rectangular "trapping region" [35] bounded by $a_{\min}^2 = -4c_0 - 2c_1$ and $a_{\max}^2 = -4c_0 + 2c_1$. These bounds are shown as the gray shaded area in the top panel. When $\omega = 1.93$ and $\omega = 2.055$ (before and after the saddle-node bifurcations), there are no fixed points in the trapping region, and therefore the trapping region contains a whirling orbit bounded by $a_{\min}$ and $a_{\max}$. This is consistent with Figs. 2 and 4, where the response amplitudes are trapped in the range $[\sqrt{2}, \sqrt{6}]$.

Let us examine the temporal characteristics of the whirling orbit. The second of Eqs. (16) is a differential equation for γ which is independent of a. Depending on c_1 and σ, there can be a range of γ for which its phase flow is fast, and a range that is slow. In the lower part of Fig. 4, in panel 1 (negative σ) the slow interval is $-\pi < \gamma < 0$, while in panel 6 (positive σ) the slow interval is $0 < \gamma < \pi$. In both cases, the γ flow is fast
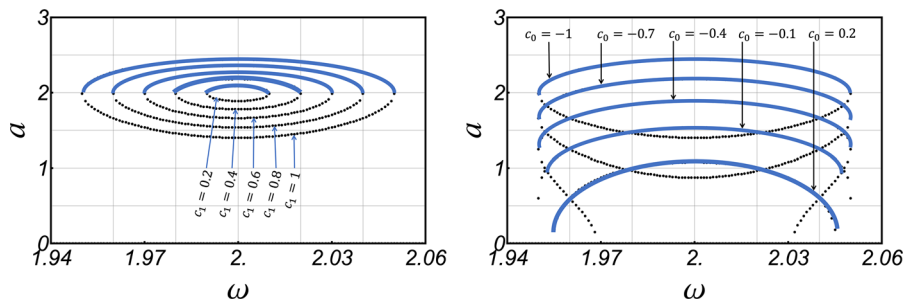
Fig. 3 PDVDP with parametric excitation only: nonzero steady-state response amplitude versus the excitation frequency in the case of subharmonic resonance where $\omega_n = 1$, $\epsilon = 0.1$, and $\alpha = $ 1, from Eq. (17). Left: $c_0 = -1$ and $c_1 = \{0.2, 0.4, 0.6, 0.8, 1\}$. Right: $c_1 = 1$ and $c_0 = \{-1, -0.7, -0.4, -0.1, 0.2\}$. Solid and dotted curves are stable and unstable branches, respectively
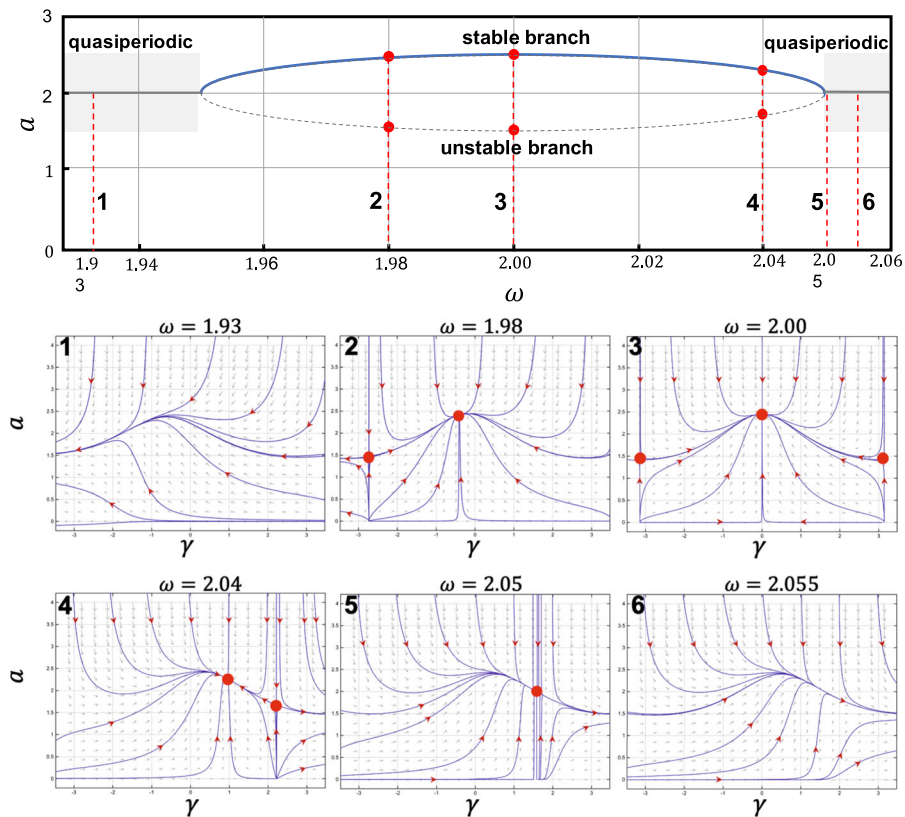

Fig. 4 PDVDP with parametric excitation only. Top panel: steady-state response amplitude versus excitation frequency close to the subharmonic resonance. Bottom panel: amplitude-phase trajectories at different corresponding frequencies $\omega = $ $\{1.93, 1.98, 2, 2.04, 2.05, 2.055\}$. The simulation parameters are $\epsilon = 0.1$, $\omega_n = 1$, $c_0 = -1$, $c_1 = 1$, and $\alpha = 1$. The range of the vertical axes is 0 to 4, and the range of the horizontal axes is $-\pi$ to π

to $a_{\max}$ and slow to $a_{\min}$, somewhat like a relaxation oscillation. This effect can be seen in Fig. 2, for the cases of $\omega = 1.93$ and $\omega = 2.055$, where the response amplitudes decrease slowly to $a = \sqrt{2}$, and increase quickly to the maximum amplitude near $a = \sqrt{6}$.

The second of Eq. (16) is independent of a and is separable. It can be integrated to obtain T_1 as a function of γ. For example, when $\sigma > 0$, a cycle is completed from $\gamma = -\pi$ to $\gamma = \pi$. These conditions can be used to determine the integration constants. As a result, and

accounting for $T_1 = \epsilon t$, the period of whirling is

$$T_{\text{est}} = \frac{2\pi\epsilon}{\sigma\sqrt{1 - (c_1/2\sigma)^2}}, \tag{20}$$

which is an estimate, since the slow flow of Eq. (16) was obtained through an asymptotic perturbation expansion. Using this expression, the period of beating of the solutions depicted in Fig. 2 is $T_{\text{est}} = 128$ (nondimensional) compared to the observed $T = 135$ for the case of $\omega = 1.93$, and $T_{\text{est}} = 225$ compared to the observed $T = 274$ for the case of $\omega = 2.055$.

Since $2\beta = \sigma T_1 - \gamma$, the leading-order solution is

$$\begin{aligned}
x_0 &= a(T_1)\cos(\omega_n T_0 + \beta(T_1)) \\
&= a(T_1)\cos\left(\frac{1}{2}(\omega T_0 - \gamma(T_1))\right).
\end{aligned} \tag{21}$$

Thus, at subharmonic resonance, the response has a reference frequency at half the forcing frequency, with amplitude and phase fluctuations. When $1.95 < \omega < 2.05$ and there is a stable fixed point in (a, γ), the steady-state solution has a fixed amplitude and phase and is phase locked. Otherwise the oscillator is in phase drift: when $\omega < 1.95$ the decreasing phase whirl increases the mean frequency, and when $\omega > 2.05$ the increasing phase whirl decreases the mean frequency, by an estimated amount $2\pi/T_{\text{est}}$, while the amplitude fluctuates.

3.3 Comments

In the perturbation analysis of the system with no external forcing, we have only detected a subharmonic resonance. The first-order perturbation analysis does not reveal a primary or superharmonic resonance. Similarly, the frequency sweep (Fig. 1) does not indicate such resonant activity for the simulated parameters.

4 Parametric and external excitation

In this case, the external forcing terms f_0 and f_1 are nonzero. Similar to the previous case, as a survey of the possible dynamics, Fig. 5 shows a frequency sweep from $\omega = 0$ to beyond $\omega = 3\omega_n$, with parameters $\omega_n = 1$, $c_0 = -1$, $c_1 = 1$, $f_0 = 0.2$, and $f_1 = 1$ when $\alpha = 1$. The sweep is based on numerical simulations and the steady-state response amplitudes are plotted. The plot shows that significant quasiperiodic dynamics occur for a large range of excitation frequencies

with periodic windows around $\omega \approx \omega_n$, $\omega \approx 2\omega_n$, and $\omega \approx 3\omega_n$. The largest responses occur near the primary resonance range. The expanded windows show details of responses within subharmonic and superharmonic resonances.

In this case, the particular solution to the leading order Eq. (3) is

$$\begin{aligned}
x_0(T_0, T_1) &= \Gamma + i\Lambda e^{i\omega T_0} \\
&+ A(T_1)e^{i\omega_n T_0} - i\Lambda e^{-i\omega T_0} + \bar{A}(T_1)e^{-i\omega_n T_0}, \tag{22}
\end{aligned}$$

where $\Gamma = \frac{f_0}{\omega_n^2}$ and $\Lambda = \frac{f_1}{2(\omega^2 - \omega_n^2)}$. By plugging Eq. (22) into (4), we obtain

$$\begin{aligned}
D_0^2 x_1 + \omega_n^2 x_1 &= (-2i\omega_n A' - ic_0\omega_n A - i\alpha\omega_n\Gamma^2 A \\
&- i\alpha\omega_n A^2\bar{A} - 2\alpha i\omega_n\Lambda^2 A)e^{i\omega_n T_0} \\
&+ (c_0\omega\Lambda + \omega\alpha\Gamma^2\Lambda + \omega\alpha\Lambda^3 + 2\alpha\omega A\bar{A}\Lambda)e^{i\omega T_0} \\
&+ \left(\frac{c_1}{2}\omega\Lambda + 2i\alpha\omega\Gamma\Lambda^2\right)e^{2i\omega T_0} \\
&- \alpha\omega\Lambda^3 e^{3i\omega T_0} + (i\frac{c_1}{2}\omega_n\bar{A} - 2\omega_n\alpha\Lambda\Gamma\bar{A} \\
&+ 2\omega\alpha\Lambda\Gamma\bar{A})e^{i(\omega-\omega_n)T_0} \\
&+ i\alpha(2\omega - \omega_n)\Lambda^2\bar{A}e^{i(2\omega-\omega_n)T_0} \\
&+ \alpha(\omega - 2\omega_n)\Lambda\bar{A}^2 e^{i(\omega-2\omega_n)T_0} + c.c. + \text{N.S.T.} \tag{23}
\end{aligned}$$

The right-hand side of Eq. (23) shows different cases of resonance; each produces different secular terms. Among all of the resonances in Eq. (23), we obtain the following solvability conditions.

1. Nonresonant:

$$\begin{aligned}
&-2i\omega_n A' - ic_0\omega_n A - i\alpha\omega_n\Gamma^2 A - i\alpha\omega_n A^2\bar{A} \\
&-2\alpha i\omega_n\Lambda^2 A = 0 \tag{24}
\end{aligned}$$

2. Primary resonance ($\omega = \omega_n + \epsilon\sigma$):

$$\begin{aligned}
&-2i\omega_n A' - ic_0\omega_n A - i\alpha\omega_n\Gamma^2 A \\
&-i\alpha\omega_n A^2\bar{A} - 2\alpha i\omega_n\Lambda^2 A \\
&+(c_0\omega\Lambda + \omega\alpha\Gamma^2\Lambda + \omega\alpha\Lambda^3 \\
&+2\alpha\omega A\bar{A}\Lambda + i(2\omega \\
&-\omega_n)\alpha\Lambda^2\bar{A})e^{i\sigma T_1} = 0 \tag{25}
\end{aligned}$$

3. Subharmonic resonance of order 1/2 ($\omega = 2\omega_n + \epsilon\sigma$):

$$\begin{aligned}
&-2i\omega_n A' - ic_0\omega_n A - i\alpha\omega_n\Gamma^2 A - i\alpha\omega_n A^2\bar{A} \\
&-2\alpha i\omega_n\Lambda^2 A + (i\frac{c_1}{2}\omega_n\bar{A} \\
&+2(\omega - \omega_n)\alpha\Lambda\Gamma\bar{A})e^{i\sigma T_1} = 0 \tag{26}
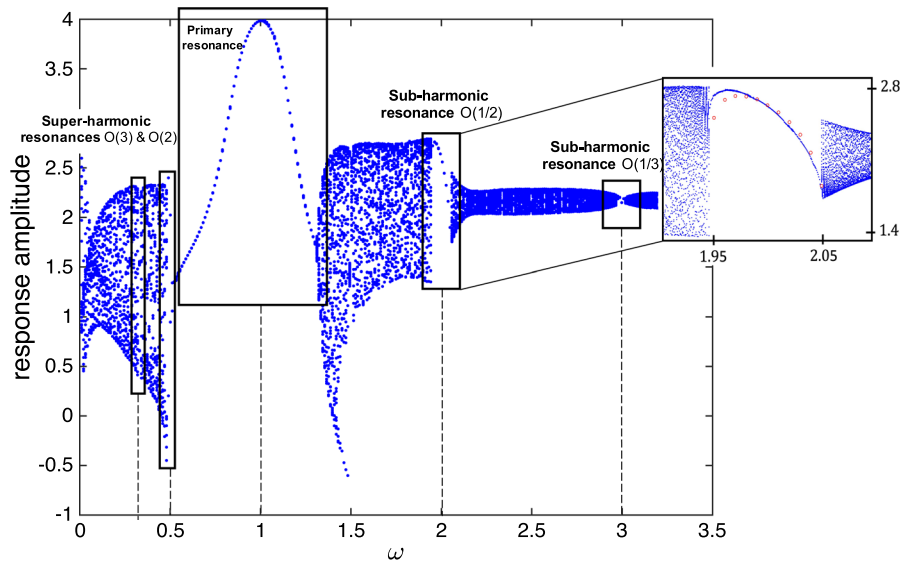\end{aligned}$$

Fig. 5 PDVDP with parametric and external excitation. The numerically solved response amplitude versus the excitation frequency ω where $f_0 = 0.2$, $f_1 = 1$, $\omega_n = 1$, $\epsilon = 0.1$, $c_0 = -1$, $c_1 = 1$, and $\alpha = 1$. Small circles in the insert are predictions from the perturbation analysis

4. Subharmonic resonance of order 1/3 ($\omega = 3\omega_n + \epsilon\sigma$):

$$-2i\omega_n A' - ic_0\omega_n A - i\alpha\omega_n\Gamma^2 A - i\alpha\omega_n A^2\bar{A}$$
$$-2\alpha i\omega_n\Lambda^2 A + (\omega - 2\omega_n)\alpha\Lambda\bar{A}^2 e^{i\sigma T_1} = 0 \quad (27)$$

5. Superharmonic resonance of order 2 ($2\omega = \omega_n + \epsilon\sigma$):

$$-2i\omega_n A' - ic_0\omega_n A - i\alpha\omega_n\Gamma^2 A - i\alpha\omega_n A^2\bar{A}$$
$$-2\alpha i\omega_n\Lambda^2 A + (\frac{c_1}{2}\omega\Lambda + 2i\omega\alpha\Gamma\Lambda^2)e^{i\sigma T_1} = 0 \quad (28)$$

6. superharmonic Resonance of Order 3 ($3\omega = \omega_n + \epsilon\sigma$):

$$-2i\omega_n A' - ic_0\omega_n A - i\alpha\omega_n\Gamma^2 A - i\alpha\omega_n A^2\bar{A}$$
$$-2\alpha i\omega_n\Lambda^2 A - \omega\alpha\Lambda^3 e^{i\sigma T_1} = 0 \quad (29)$$

Here we study cases 1, 3 and 5. Case 4 does not involve the parametric term, and case 6 is of minimal significance. However, the subharmonic of order 1/2 and the superharmonic of order 2 involve both van der Pol and parametric damping terms together. (Note that for the nonresonant case we include x_1, which is affected by c_1, discussed below.)

Although Fig. 5 indicates the primary resonance as a prominent case when $\omega \approx \omega_n$, the coefficient Λ

becomes singular and would contradict the multiple-scales bookkeeping strategy. The analysis of primary resonance case requires weak excitation, as well as a second-order perturbation analysis to capture the parametric term, as in [24]. This will be analyzed in a separate study.

4.1 Nonresonant case

The solvability condition in Eq. (24) is not affected by the parametric damping term and hence the behavior is similar to the forced van der Pol equation [3,4]. In this case, the phase equation becomes $\beta' = 0$, and hence the phase β is constant and does not influence the oscillation frequency. Equation (24) yields the following steady-state solutions

$$a = 0, \qquad a = \frac{2}{\sqrt{\alpha}}\sqrt{-c_0 - \alpha\Gamma^2 - 2\alpha\Lambda^2}, \quad (30)$$

where the zero solution is unstable and the nonzero solution exists and is stable when $\alpha\Gamma^2 + 2\alpha\Lambda^2 < -c_0$. Since $\alpha\Gamma^2 + 2\alpha\Lambda^2 > 0$, a negative value of c_0 is necessary (but not sufficient) for nonzero a. If the above condition is not satisfied, then the trivial solution $a = 0$ is stable.

Since the leading-order solution has the form

$$x_0 = \Gamma - 2\Lambda \sin \omega T_0 + a \cos(\omega_n T_0 + \beta) \qquad (31)$$

when the condition $\alpha\Gamma^2 + 2\alpha\Lambda^2 < -c_0$ is satisfied, $a \neq 0$ and the response becomes quasiperiodic. Otherwise, with sufficient increase in the excitation (Λ and Γ), a is suppressed and the response becomes periodic, known as quenching [3,4].

The parametric terms affect the first-order correction, x_1, in the approximate solution $x(t) = x_0(t_0, T_1) + \epsilon x_1(T_0, T_1)$, similar to what was seen in the unforced case. In eliminating the secular terms, there are several contributions of different frequency components, including 2ω, $\omega - \omega_n$, $\omega + \omega_n$, from parametric excitation and van der Pol terms, and $2\omega_n$, $3\omega_n$, 3ω, $2\omega - \omega_n$, $2\omega + \omega_n$, $\omega - 2\omega_n$, and $\omega + 2\omega_n$, from the van der Pol terms. Thus the first-order correction, x_1, can contribute additional two-frequency quasiperiodic effects which depend on parametric damping c_1, and the content of the total response has linear combinations of two independent frequencies.

The numerical solutions in Fig. 6 demonstrate that when $\omega = 0.12$, the response is quasiperiodic. This is consistent with the leading-order solution presented in Eq. (31). Also shown in the figure are solutions near subharmonic resonance, which is discussed in the next section.

4.2 Subharmonic resonance of order 1/2

In this case, the excitation and natural frequencies are related as $\omega = 2\omega_n + \epsilon\sigma$. We see from the solvability condition in Eq. (26) that in addition to the nonresonant secular terms in Eq. (24), the parametric damping and forcing appear. We substitute $A(T_1) = \frac{1}{2}a(T_1)e^{i\beta(T_1)}$ into the equation and let $\gamma = \sigma T_1 - 2\beta$. Then, the autonomous coupled system of governing equations of the amplitude a and phase γ becomes

$$a' + \frac{1}{8}\alpha a^3 + \left(\frac{c_0}{2} + \frac{\alpha\Gamma^2}{2}\right.$$
$$\left. + \alpha\Lambda^2 - \frac{c_1}{4}\cos\gamma + \alpha\Gamma\Lambda(1 - \frac{\omega}{\omega_n})\sin\gamma\right)a = 0,$$
$$a\gamma' - a\sigma + \frac{c_1}{2}a\sin\gamma + 2a\alpha\Gamma\Lambda(1 - \frac{\omega}{\omega_n})\cos\gamma = 0. \qquad (32)$$

The fixed points of Eqs. (32) are obtained in the steady-state case when $a' = \gamma' = 0$, which admits $a = 0$ and

a nontrivial solution. The equations for the nontrivial solution take the form

$$A_1 \sin\gamma + B_1 \cos\gamma = C_1, \quad A_2 \sin\gamma + B_2 \cos\gamma = C_2,$$

where the coefficients A_1, A_2, B_1, B_2, C_1, and C_2 are functions of the parameters and the amplitude a (increasing α reduces the steady-state amplitudes, a). By solving for $\sin\gamma$ and $\cos\gamma$, and using the trigonometric identities, we can first obtain the phase, and then we remove the variable γ and form an algebraic equation to obtain the steady-state amplitude a as,

$$\alpha^2 a^4 + 8a^2(\alpha c_0 + 2\alpha^2\Lambda^2 + \alpha^2\Gamma^2)$$
$$+ 4\left(4c_0^2 + 16\alpha c_0\Lambda^2 - c_1^2 + 16\alpha^2\Lambda^4 + 4\sigma^2\right)$$
$$+ 16\Gamma^2\left(2\alpha c_0 - 4\alpha^2\Lambda^2 \frac{\omega}{\omega_n}(\frac{\omega}{\omega_n} - 2) + \alpha^2\Gamma^2\right) = 0. \qquad (33)$$

Solving for a^2 yields

$$a^2 = -4\left(\frac{c_0}{\alpha} + \Gamma^2 + 2\Lambda^2\right)$$
$$\pm 2\Gamma\Lambda\sqrt{\frac{(c_1^2 - 4\sigma^2)}{\alpha^2\Gamma^2\Lambda^2} + \frac{16(\omega - \omega_n)^2}{\omega_n^2}}\right), \qquad (34)$$

which is valid if the square root in the solution is real, and if $a^2 \geq 0$. The first criterion reduces to $4\sigma^2 < c_1^2 + 16\alpha^2\Gamma^2\Lambda^2$, when using $\omega - \omega_n \approx \omega_n$. Thus the frequency range of fixed amplitude solutions increases with c_1, f_0, and f_1.

Based on Eq. (31) and the definition of γ, the leading order solution takes the form

$$x_0 = \Gamma - 2\Lambda \sin(\omega T_0) + a \cos\left(\frac{\omega}{2}T_0 - \frac{\gamma}{2}\right). \qquad (35)$$

For the case when a and γ are fixed and stable, there is a periodic (phase locked) response of fundamental frequency $\omega/2$. When a steady-state solution a does not exist, the response is in phase drift and is quasiperiodic.

Figure 7 shows the steady-state response amplitude versus the excitation frequency for small values of detuning parameter, when $\epsilon = 0.1$ and $-\sigma_0 < \sigma < \sigma_0$, where $\sigma_0 = 0.5$. Note that these figures show the amplitude a of one term in Eq. (35). The phase γ would affect peak-to-peak amplitudes. The mean damping and periodic forcings are set to be constant, $c_0 = -1$ and $f_1 = 1$, while different values of $c_1 = \{0.2, 0.5, 1\}$ produce different closed curves. The larger values of c_1 are associated with the larger ovals. We see that as the constant forcing term f_0 is increasing between $\{0.2, 0.4, 0.6\}$, the ovals are expanding and the limit cycle amplitude
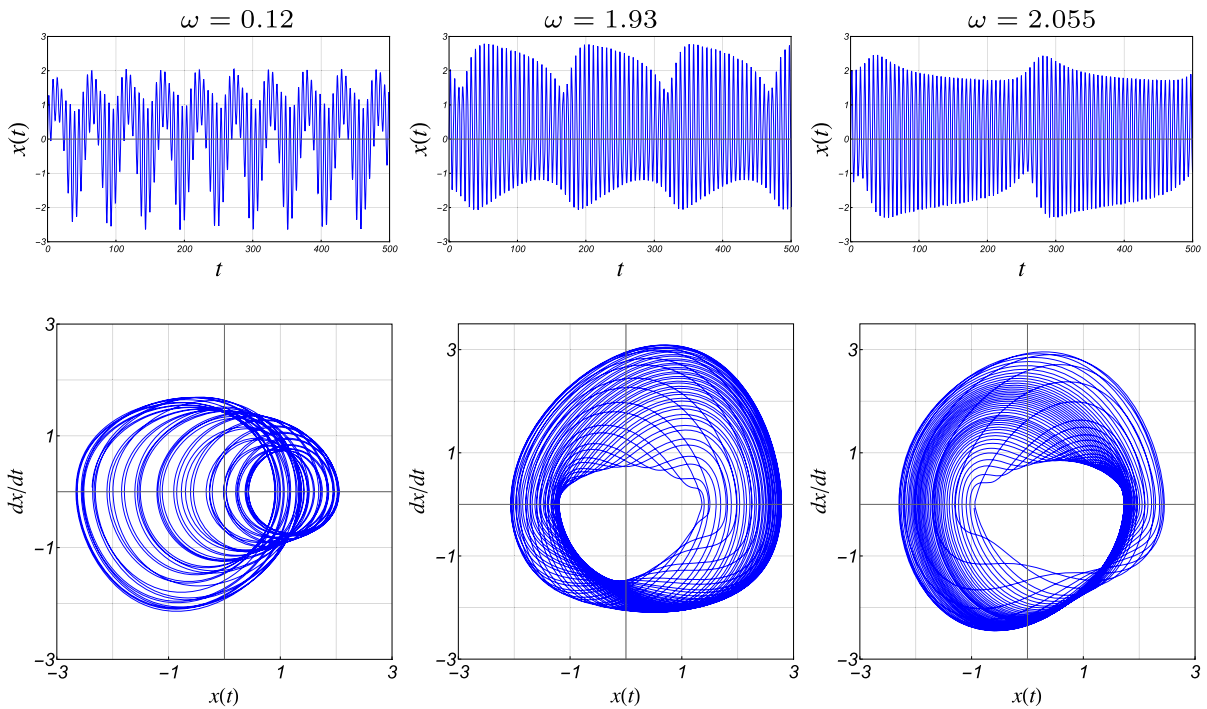
Fig. 6 PDVDP with parametric and direct excitation: numerically solved time response (top row) and phase portrait (bottom row) at different excitation frequencies where $f_0 = 0.2$ and $f_1 = 1$, $\omega_n = 1$, $\epsilon = 0.1$, $c_0 = -1$, $c_1 = 1$, and $\alpha = 1$
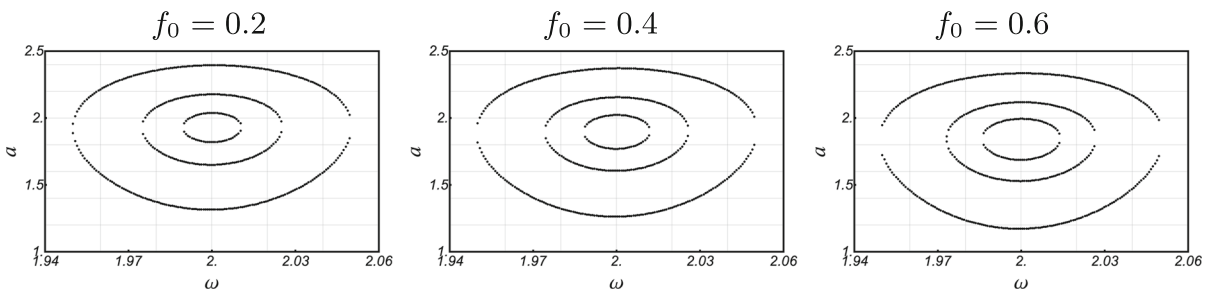

Fig. 7 PDVDP with parametric and external excitation in the case of subharmonic resonance where $\omega_n = 1$, $\alpha = 1$, $\epsilon = 0.1$, $c_0 = -1$, and $f_1 = 1$. The three plotted curves correspond to $c_1 = \{0.2, 0.5, 1\}$, and the panels are for $f_0 = \{0.2, 0.4, 0.6\}$. Upper and lower curves are stable and unstable branches, respectively. The larger values of c_1 produce the larger ovals

decreases, both very slightly. The upper curves represent the stable responses and the lower curves are the unstable responses. The stable upper curves represent responses with constant a and γ, and considering the leading order solution of Eq. (35), responses are phase locked. Outside the interval of the closed curve, a and γ are not fixed, and we have phase drift.

Figure 6 shows two numerical phase-drift solutions near subharmonic resonance. Like the unforced case, $\omega = 1.93$ and $\omega = 2.055$ are outside the interval of

the subharmonic phase locking, as seen in the insert of Fig. 5. The analytical estimates of amplitude, and phase as well, for the phase-locked case, can be inserted into Eq. (35) to estimate the total response amplitude. Samples within $1.95 < \omega < 2.05$ are plotted as circles in the insert of Fig. 5.

Figure 8 shows the dynamics of the amplitude and phase for the forced excitation, represented by Eqs. (32). The behavior is similar to the unforced case. For $\sigma < \sigma_0$, a whirling solution travels from right
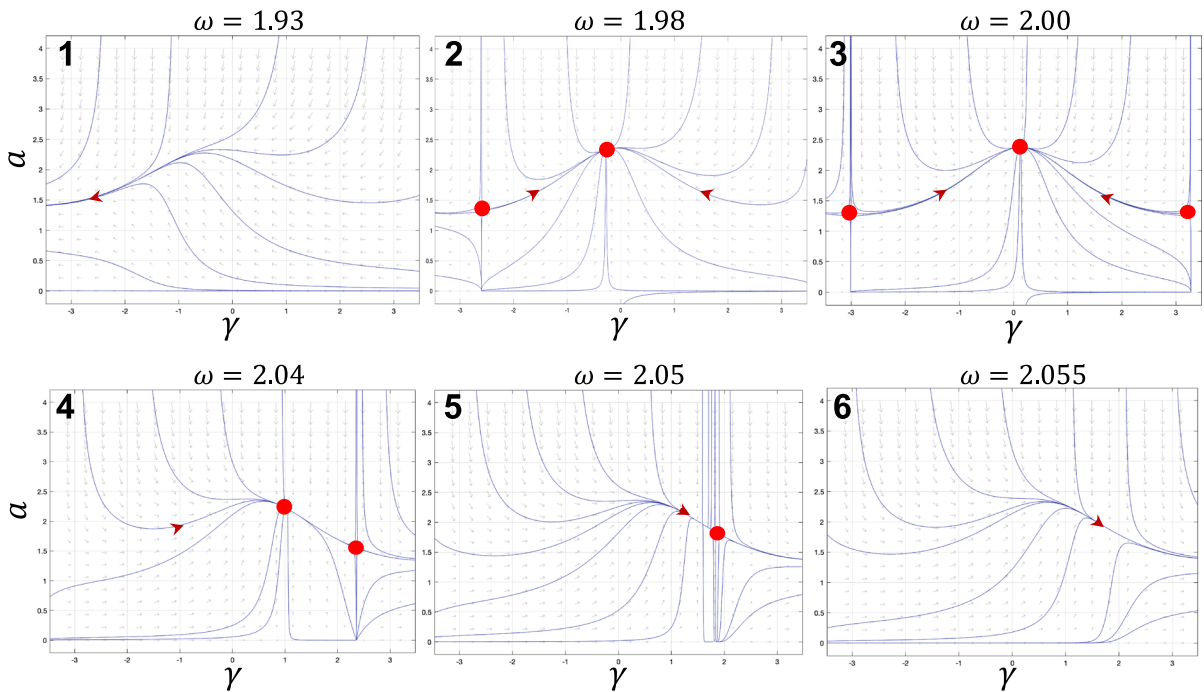
Fig. 8 PDVDP with parametric and direct excitation. Amplitude-phase trajectories at different corresponding frequencies $\omega = \{1.93, 1.98, 2, 2.04, 2.05, 2.055\}$. The simulation parameters are $\epsilon = 0.1$, $\omega_n = 1$, $c_0 = -1$, $c_1 = 1$, and $\alpha = 1$. The range of the vertical axes is 0 to 4, and the range of the horizontal axes is $-\pi$ to π

to left, and for $\sigma > \sigma_0$ the whirling solution travels from left to right. Therefore, in the leading order solution the amplitude a has a periodic fluctuation, and the oscillator is quasiperiodic. If $4\sigma^2 < c_1^2 + 16\alpha^2\Gamma^2\Lambda^2$ there exists a nonzero response amplitude. For all σ there is a trapping region $[a_{\min}, a_{\max}]$, obtained from the first of Eqs. (32) as $a_{\min} = 1.27$ and $a_{\max} = 2.38$ for the given parameters. These values are consistent with Figs. 8 and 6. The second of Eqs. (32) is used to find the time characteristics of the whirling orbit of the system with the external excitation. For a complete cycle, from $\gamma = -\pi$ to $\gamma = \pi$, T_{est} is calculated. Considering $T_1 = \epsilon t$, the estimated period of whirling for the case of panel 6 in Fig. 8 is $T_{\text{est}} = 286.1$ compared to the observed $T = 241$ in Fig. 6.

By considering Eqs. (32), we can argue that if there are no fixed points in (a, γ), we can expect whirling, where the leading order solution (Eq. 35) includes a time varying amplitude a, limited by $[a_{\min}, a_{\max}]$ of the trapping region, and phase γ, and as such the response will be quasiperiodic. In contrast, when there is a stable fixed point in (a, γ), the response becomes phase locked and periodic. The subharmonic behavior of the

parametric plus direct excitation is thus similar to that of the parametric excitation only, although the solutions for the steady amplitudes are more complicated and distorted by the direct excitation terms f_0 and f_1.

4.3 Superharmonic resonance of order 2

In this case, the excitation and natural frequency are related as $2\omega = \omega_n + \epsilon\sigma$. Similar to the subharmonic resonance, we see from the solvability condition in Eq. (28) that in addition to the nonresonant secular terms in Eq. (24), the parametric damping and forcing terms are present. $A(T_1) = \frac{1}{2}a(T_1)e^{i\beta(T_1)}$ is substituted into the equation. Letting $\gamma = \sigma T_1 - \beta$, the coupled system of governing equations of the amplitude a and phase γ becomes

$$a' + \frac{1}{8}\alpha a^3 + \left(\frac{c_0}{2} + \frac{1}{2}\alpha\Gamma^2 + \alpha\Lambda^2\right)a$$
$$-2\alpha\Gamma\Lambda^2\frac{\omega}{\omega_n}\cos\gamma - \frac{1}{2}c_1\Lambda\frac{\omega}{\omega_n}\sin\gamma = 0,$$
$$a\gamma' - a\sigma + 2\alpha\Gamma\Lambda^2\frac{\omega}{\omega_n}\sin\gamma$$
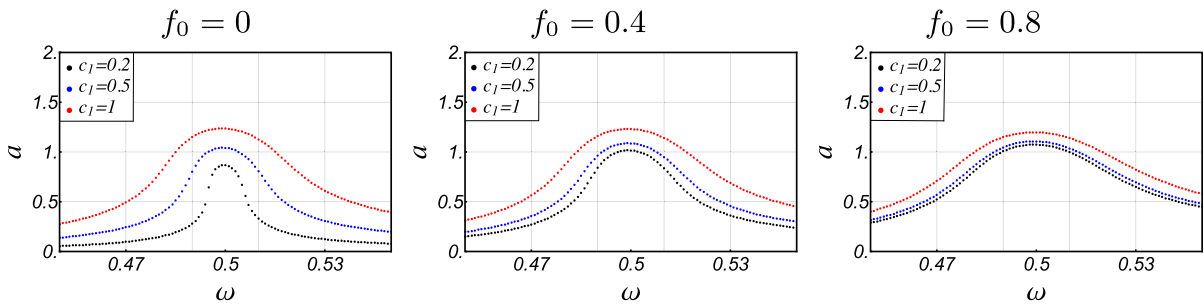
Fig. 9 PDVDP with parametric and external excitation. Steady-state response amplitude versus the excitation frequency in the case of superharmonic resonance where $\omega_n = 1, \alpha = 1, \epsilon = 0.1,$ $c_0 = -1,$ and $f_1 = 1.$ The three plotted curves correspond to $c_1 = \{0.2, 0.5, 1\},$ and the panels are for $f_0 = \{0, 0.4, 0.8\}$

$$-\frac{1}{2}c_1\Lambda\frac{\omega}{\omega_n}\cos\gamma = 0. \tag{36}$$

For the superharmonic case, the fixed points are found by setting $a' = \gamma' = 0$ in Eqs. (36). By taking a similar approach as in the subharmonic case, an algebraic expression relating the steady-state amplitude a to parameters can be obtained as

$$\frac{a^2\omega_n{}^2\left(\left(4c_0 + \alpha(a^2 + 4\Gamma^2 + 8\Lambda^2)\right)^2 + 64\sigma^2\right)}{16\Lambda^2\omega^2\left(16\alpha^2\Gamma^2\Lambda^2 + c_1{}^2\right)} = 1. \tag{37}$$

Figure 9 demonstrates the steady-state response amplitude for varying values of excitation frequencies where $\omega_n = 1,$ $\alpha = 1,$ $\epsilon = 0.1,$ $c_0 = -1,$ $c_1 = \{0.2, 0.5, 1\},$ and $f_0 = \{0, 0.4, 0.8\}.$ Marching from the upper curves to the lower curves the value of c_1 is descending. Increasing f_0 increases the amplitude of the response such that the curves with lower values of c_1 are expanded more.

As seen in Fig. 5, the superharmonic window is slender and yields to dominant primary resonance curve. We looked at numerical solutions in a magnified superharmonic sweep window (not shown here) and observed that the superharmonic phase locking occurring at $\omega \approx 0.5$ has very weak (slow) stability, reducing its observation in the full system. Slightly below the superharmonic condition, it is likely that the perturbation of the slow flow overcomes its weak asymptotic solution, and apparently quasiperiodic behavior is observed. The mechanism for how the primary resonance curve dominates above the superharmonic will be examined when primary resonance is studied later.

5 Brief examination of strong nonlinearity

The response of the system in Eq. (1) varies significantly when the nonlinearity becomes stronger, i.e., when ϵ increases. If ϵ is large enough, the perturbation analysis is no longer valid. We resort to numerical simulations by using the method explained in Sect. 3. Figure 10 shows a frequency sweep with $\omega \in [0, 3.5]$ for different values of $\epsilon \in [0.01, 3]$, where $c_0 = -1,$ $c_1 = 1,$ and $\alpha = 1.$ At each frequency, the simulation begins at the same initial conditions. While it is possible that multiple steady-state solutions coexist, only one solution is obtained at each frequency. Significant changes in the response can be observed at different frequencies as ϵ takes larger values. This figure suggests the possibility of chaotic behavior in the presence of strong nonlinearity. In particular, Fig. 11 illustrates time responses and phase portraits of the system with large nonlinearity and suggests intermittency when $\epsilon = 2$ and $\omega = 3.2.$

6 Summary and conclusion

In this paper, we studied the responses of a forced and unforced van der Pol equation with parametric damping. The first-order method of multiple scales and numerical solutions were used. Applications can include vertical-axis wind turbine blade vibration, which can have parametric damping and van-der-Pol type terms in simplified models.

The parametric damping with no external excitation was analyzed in nonresonant and subharmonic resonance cases. The system shows an oscillatory quasiperiodic behavior in the former case. In the latter

Fig. 10 PDVDP with
parametric and direct
excitation: amplitude versus
excitation frequency for
different values of ϵ, where
$f_0 = 0.2$ and
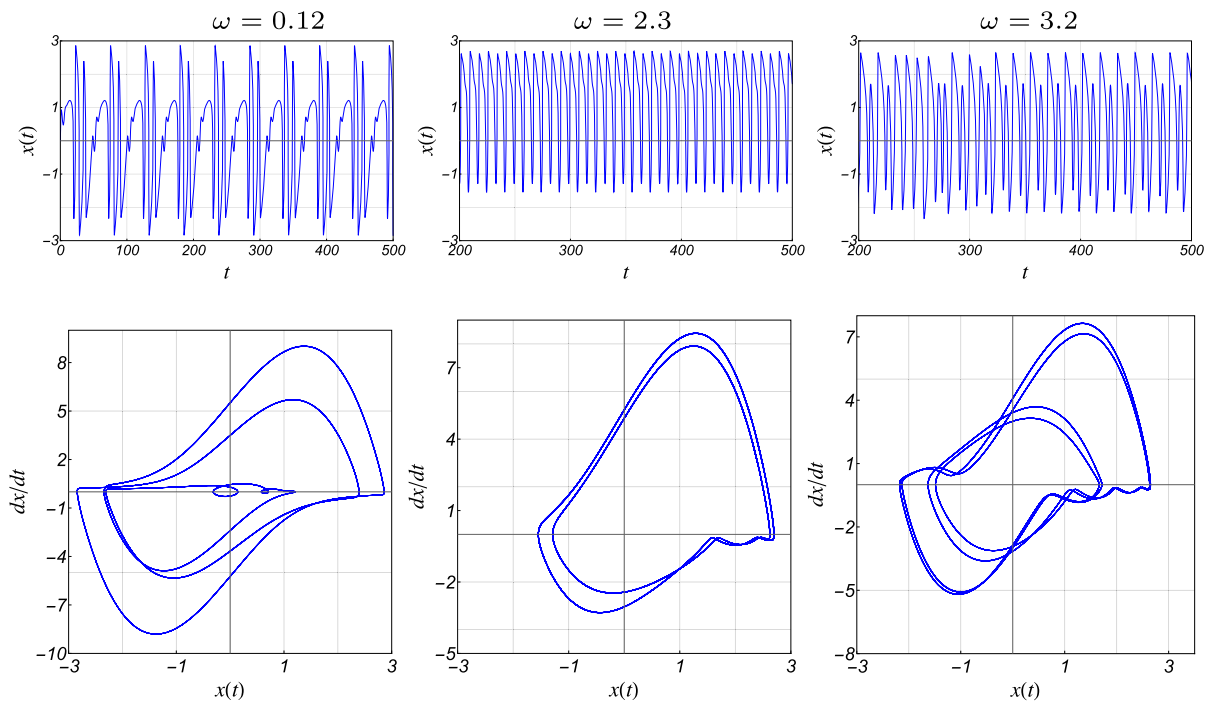$f_1 = 1, \omega_n = 1, c_0 = -1$,
$c_1 = 1$, and $\alpha = 1$
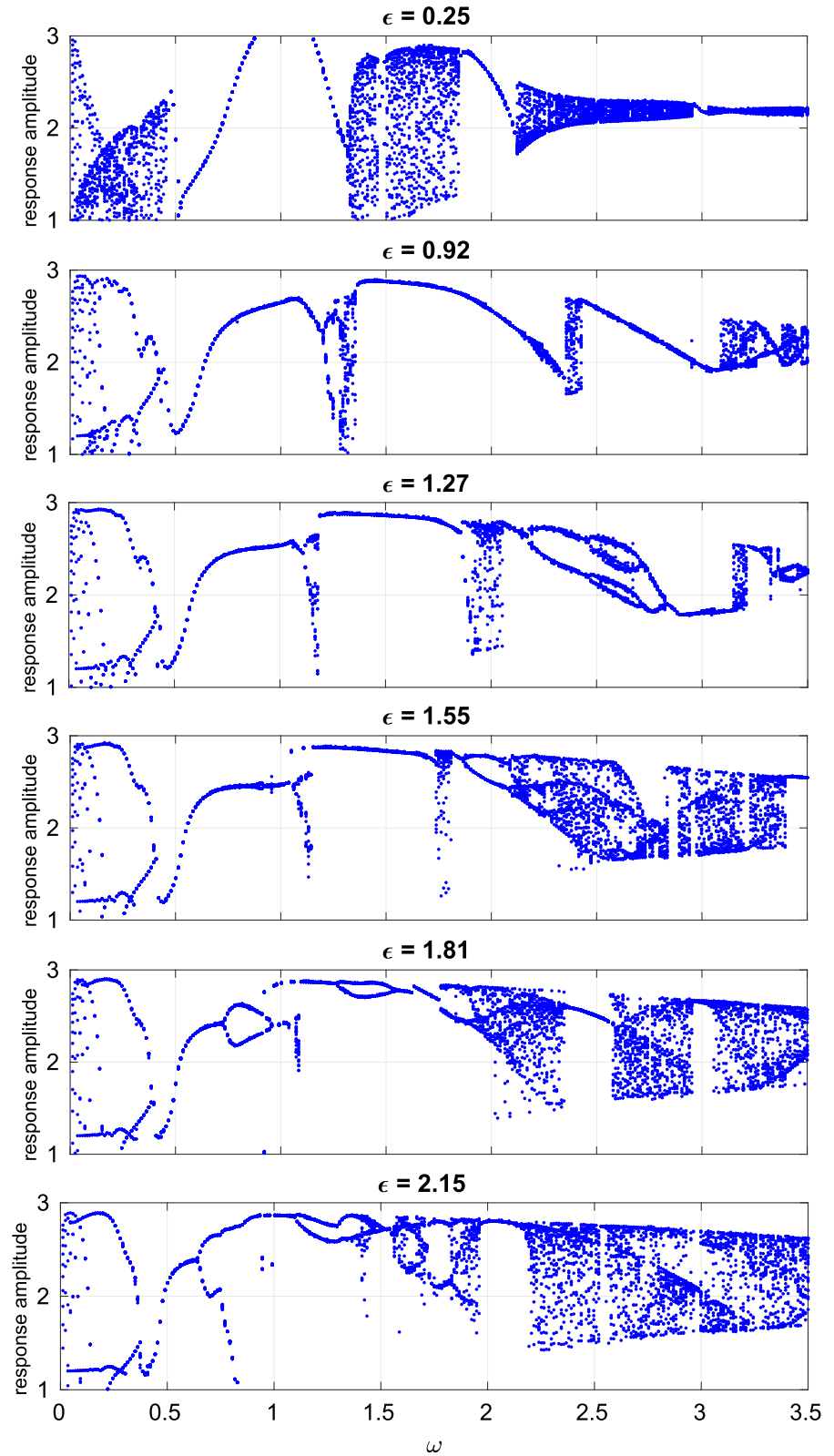
Fig. 11 PDVDP with parametric and direct excitation: time response (top row) and phase portrait (bottom row) at different excitation frequencies where $f_0 = 0.2$ and $f_1 = 1$, $\omega_n = 1$, $\epsilon = 2$, $\alpha = 1$, $c_0 = -1$ and $c_1 = 1$

resonance case, we found the steady-state amplitude versus the excitation frequency for different damping parameters. When $c_0 = -1$ (negative linear damping as with the van der Pol oscillator), the resonant response amplitude increases with the parametric damping c_1. An increase in the mean value of damping c_0 (i.e., making c_0 less negative) decreases the response amplitude. The dynamics of the amplitude and phase showed saddle-node bifurcations coinciding with the onset of phase locking, in which periodically whirling amplitude and phase (quasiperiodic oscillations) were replaced with a fixed steady-state amplitude and phase (periodic oscillations). In the phase drift case, the period of amplitude fluctuations could be estimated.

We then studied the parametrically damped van der Pol equation with direct excitation. In the nonresonant case, the parametric damping term does not contribute in the solvability condition and therefore it showed similar behavior as the forced van der Pol oscillator. The nonresonant system can exhibit the quenching phenomenon when the excitation through the mean or cyclic direct forcing is sufficiently large.

The subharmonic resonance behavior was similar to that of the parametric excitation without direct excita-

tion, except that the direct excitation terms complicate and distort the steady solutions. Saddle-node bifurcations in the slow flow corresponded to transitions to phase locking. The phase-drift amplitude-fluctuation period was estimated. Increasing the parametric damping parameter, c_1, increases the steady-state amplitude, and the direct forcing, f_0 and f_1 perturbed the amplitude curve.

In addition to the nonresonant and subharmonic resonance, the parametrically damped van der Pol oscillator with direct excitation experienced superharmonic resonance. It was shown that the amplitude of the response increases with c_1, f_0, and f_1.

Our numerical studies showed the primary resonance as a dominant forced response case. The analysis of this case requires further investigation that will be done as a subsequent study with weak excitation. Based on previous studies on the cases with forcing and cyclic stiffness [24,36], we expect that a second-order multiple-scales analysis should be considered to correctly pull out the contribution of the parametric damping to the different resonance cases.

Numerical studies with strong nonlinearity suggested responses with many harmonics and chaos are possible.

Data availability statement The datasets generated during and/or analyzed during the current study are available from the corresponding author on reasonable request.

Declarations

Conflict of interest The authors declare that they have no conflict of interest.

References

1. Afzali, F., Kapucu, O., and Feeny, B. F.: Vibrational analysis of vertical-axis wind-turbine blades. In: Proceedings of the ASME 2016 International Design Engineering Technical Conferences. Paper number IDETC2016-60374, Charlotte, North Carolina (2016)
2. Afzali, F., Acar, G.D., Feeny, B.F.: A Floquet-based analysis of parametric excitation through the damping coefficient. J. Vib. Acoust. **143**, 4 (2020)
3. Nayfeh, A.H., Mook, D.T.: Nonlinear Oscillations. Wiley, New York (2008)
4. Rand, R.H.: Lecture notes on nonlinear vibrations. https://ecommons.cornell.edu/handle/1813/28989 (2012)
5. van der Pol, B.: The nonlinear theory of electrical oscillations. Proc. IRE **22**(9), 1051–1086 (1934)
6. Holmes, P.J., Rand, D.A.: Bifurcations of the forced van der Pol oscillator. Q. Appl. Math. **35**(4), 495–509 (1978)
7. Barbosa, R.S., Machado, J.T., Vinagre, B., Calderon, A.: Analysis of the van der Pol oscillator containing derivatives of fractional order. J. Vib. Control **13**(9–10), 1291–1301 (2007)
8. Náprstek, J., Fischer, C.: Super and sub-harmonic synchronization in generalized van der Pol oscillator. Comput. Struct. **224**, 106103 (2019)
9. Barrón, M.A., Sen, M.: Synchronization of four coupled van der Pol oscillators. Nonlinear Dyn. **56**(4), 357–367 (2009)
10. Ward, M.: Lecture Notes on Basic Floquet Theory. http://www.emba.uvm.edu/jxyang/teaching/ (2010)
11. Hartono, Burgh, A.H.P.: An Equation Time-Periodic Damping Coefficient: Stability Diagram and an Application. Delft University of Technology, Delft (2002)
12. Acar, G., Feeny, B.F.: Floquet-based analysis of general responses of the Mathieu equation. J. Vib. Acoust. **138**(4), 0410179 (2016)
13. Afzali, F., Feeny, B.F.: Response characteristics of systems with parametric excitation through damping and stiffness. In: ASME International Design Engineering Technical Conferences and Computers and Information in Engineering Conference, American Society of Mechanical Engineers. paper number DETC2020-22457 (2020)
14. Month, L., Rand, R.H.: Bifurcation of 4–1 subharmonics in the nonlinear Mathieu equation. Mech. Res. Commun. **9**(4), 233–240 (1982)
15. Ng, L., Rand, R.H.: Bifurcations in a Mathieu equation with cubic nonlinearities. Chaos Solitons Fractals **14**(2), 173–181 (2002)
16. Tondl, A., Ecker, H.: On the problem of self-excited vibration quenching by means of parametric excitation. Appl. Mech. **72**, 923–932 (2003)
17. Veerman, F., Verhulst, F.: Quasiperiodic phenomena in the van der Pol–Mathieu equation. J. Sound Vib. **326**(1–2), 314–320 (2009)
18. Rugar, D., Grutter, P.: Mechanical parametric amplification and thermomechanical noise squeezing. Phys. Rev. Lett. **67**(6), 699–702 (1991)
19. Guennoun, K., Houssni, M., Belhaq, M.: Quasiperiodic solutions and stability for a weakly damped nonlinear quasiperiodic Mathieu equation. Nonlinear Dyn. **27**(3), 211–236 (2002)
20. Rhoads, J.F., Shaw, S.W.: The impact of nonlinearity on degenerate parametric amplifiers. Appl. Phys. Lett. **96**(23), 234101 (2010)
21. Ramakrishnan, V., Feeny, B.F.: Resonances of a forced Mathieu equation with reference to wind turbine blades. J. Vib. Acoust. **134**(6), 064501 (2012)
22. Inoue, T., Ishida, Y., Kiyohara, T.: Nonlinear vibration analysis of the wind turbine blade (occurrence of the superharmonic resonance in the out of plane vibration of the elastic blade). J. Vib. Acoust. **134**(3), 031009 (2012)
23. Sharma, A.: A re-examination of various resonances in parametrically excited systems. J. Vib. Acoust. **142**(3), 03101011 (2020)
24. Ramakrishnan, V., Feeny, B.F.: Primary parametric amplification in a weakly forced Mathieu equation. J. Vib. Acoust. **144**(5), 051006 (2022)
25. Goswami, I., Scanlan, R.H., Jones, N.P.: Vortex-induced vibration of circular cylinders. ii: New model. J. Eng. Mech-Asce. **119**(11), 2288–2302 (1993)
26. Pandey, M., Rand, R.H., Zehnder, A.T.: Frequency locking in a forced Mathieu–van-der-Pol–Duffing system. Nonlinear Dyn. **54**(1–2), 3–12 (2008)
27. Belhaq, M., Fahsi, A.: 2: 1 and 1: 1 frequency-locking in fast excited van der Pol-Mathieu-Duffing oscillator. Nonlinear Dyn. **53**(1), 139–152 (2008)
28. Szabelski, K., Warmiński, J.: Parametric self-excited nonlinear system vibrations analysis with inertial excitation. Int. J. Non-Linear Mech. **30**(2), 179–189 (1995)
29. Warminski, J.: Nonlinear dynamics of self-, parametric, and externally excited oscillator with time delay: van der Pol versus Rayleigh models. Nonlinear Dyn. **99**(1), 35–56 (2020)
30. Chakraborty, S., Sarkar, A.: Parametrically excited nonlinearity in van der Pol oscillator: resonance, anti-resonance and switch. Physica D **254**, 24–28 (2013)
31. Allen, M.S., Sracic, M.W., Chauhan, S., Hansen, M.H.: Output-only modal analysis of linear time-periodic systems with application to wind turbine simulation data. Mech. Syst. Signal Process. **25**(4), 1174–1191 (2011)
32. Acar, G.D., Acar, M.A., Feeny, B.F.: Parametric resonances of a three-blade-rotor system with reference to wind turbines. J. Vib. Acoust. **142**(2), 0210139 (2020)

33. Luongo, A., Zulli, D.: Parametric, external and self-excitation of a tower under turbulent wind flow. J. Sound Vib. **330**(13), 3057–3069 (2011)

34. Nayfeh, A.H.: Perturbation Methods. Wiley, New York (2008)

35. Guckenheimer, J., Holmes, P.: Nonlinear Oscillations, Dynamical Systems, and Bifurcations of Vector Fields. Springer, New York (1983)

36. Ramakrishnan, V.: Analysis of wind turbine blade vibration and drivetrain loads. PhD thesis, Michigan State University, East Lansing (2017)